Microporous and Mesoporous Materials 267 (2018) 257–264

Contents lists available at ScienceDirect

Microporous and Mesoporous Materials

journal homepage: www.elsevier.com/locate/micromeso

Pore structure development of silica particles below the isoelectric point

A. Lazaro[a,*], K. Sato[b], H.J.H. Brouwers[a], J.W. Geus[c]

[a] Department of the Built Environment, Eindhoven University of Technology, P.O. Box 513, 5600 MB Eindhoven, The Netherlands
[b] Department of Environmental Sciences, Tokyo Gakugei University, 4-1-1 Koganei, Tokyo 184-8501, Japan
[c] Debye Institute for Nanomaterials Science, University of Utrecht, Utrecht, The Netherlands

ARTICLE INFO

Keywords:
Textural properties
Porosity
Mesoporous silica
Pore size distribution
Acid

ABSTRACT

The textural properties of amorphous silica play a fundamental role in its final properties and, therefore, in its possible applications. The aim of this study is to gain comprehensive understanding about how the process conditions influence the pore structure of silica synthesized below the isoelectric point and find possible solutions to tailor the final properties of nano-silica. This study was conducted using the mineral olivine as silica source and dissolving it in sulfuric acid. This synthesis method is an interesting and sustainable alternative to the existing commercial methods. This nano-silica exhibits a specific surface area in the range of 100–500 m^2/g and a pore size distribution of 1–100 nm for silicas with a purity above 99%. At the beginning of the reaction, silica is microporous and mesoporous, showing no macroposity. As the reaction conversion progresses, silica particles become larger and macroporous, and internal porosity is developed. The process conditions have an important influence on the textural properties of nano-silica. By modifying the process conditions the small mesopores can be removed featuring no porosity below 9 nm and the large pores can be reduced to pore sizes as small as 30 nm. The possibility of tailoring the porosity of silica in this large range makes this material suitable for a wide range of applications.

1. Introduction

Nano-silica is one of the most used nano-materials, and its use is rising 5% per year being the estimated market for specialty silicas of $8.8 billion per year in 2020 [1]. Nowadays, the two most important commercial processes in the production of nano-silica in terms of volume are the neutralization of sodium silicate solutions with acid and the flame hydrolysis of silicon tetrachloride. Both processes are expensive and not environmentally friendly because of the high temperature steps (usually above 1000 °C) involved in these processes. In addition, nano-silica prepared using the Stöber method [2] (or a modification of this) is only used when perfect control of the particle size of colloids or the pore size of mesostructure materials is required, due to its high production costs. The production of nano-silica using silicate minerals (e.g., olivine) below the isoelectric point (i.e., pH = 2) is an interesting alternative to the existing commercial methods because of the good quality of the resulting silica and low energy requirements (and low CO_2 emissions) as was demonstrated in Ref. [3–5], which makes it cheaper and more sustainable.

Silica Powder (e.g., precipitated silica and pyrogenic silica) is the most common produced form of silica, with its particle structure, pore structure and surface chemistry being the most important parameters. The pore structure of amorphous silica strongly affects the properties and functionality of silica and, therefore, its possible applications. For instance, the pore structure plays a fundamental role in catalysis, drug delivery and ultrafiltration [6–8]. In addition, the use of mesoporous materials (e.g., SBA-15 and MCM-41) with defined pore sizes has exponentially increased in the last years. These materials are usually produced using TEOS and surfactant [9–12]. At the right conditions, the surfactant produces a template where the silica deposits on. Finally the surfactant is removed at high temperatures. The pore size distribution of this type of materials depends mainly on the template used, and, therefore, their textural properties can be modified by changing the assembly of the template. Even though the porosity development of silica has been widely investigated above the isoelectric point (IEP) [13–18], there are only few studies researching about this topic below pH 2 [3,4,19,20].

The surface area and porosity of silica gels were studied using sodium silicate solutions at pH above and below the IEP by Okkerse [20], and it was concluded that the specific surface area (SSA) was mainly influenced by the size of the primary particles. Furthermore, this study stated that in the pH range between −1 and 5, the primary particle size remained constant. This constant size is because the reaction rate and reaction time have opposite effects on the primary particle size

* Corresponding author.
E-mail address: a.lazaro.garcia@tue.nl (A. Lazaro).

https://doi.org/10.1016/j.micromeso.2018.03.031
Received 17 December 2017; Received in revised form 28 February 2018; Accepted 26 March 2018
Available online 28 March 2018
1387-1811/

cancelling each other effects. Lieftink [19] studied the pore size distribution (PSD) of nano-silica synthesized by the dissolution of olivine using nitrogen physisorption and found that at low reaction conversions olivine nano-silica was microporous and mesoporous; if the reaction continues, macropores were also developed. Although this study was pioneering in the pore structure of silica below the IEP, the BJH method was the only pore size distribution method used. The BJH method is one of the most common methods used to determine the PSD because of its simplicity. However, it presents several drawbacks [21]. 1) In micropores the concept of capillary condensation is no longer valid [22]. 2) For pores narrower than 10 nm curvature effects should be considered [22,23]. 3) When the material has a random distribution of interconnected pores, the tensile strength effect occurs, which abruptly closes the hysteresis. In addition, this method can underestimates the pore size for pores narrower than 10 nm [22,24].

Furthermore, the material was degassed at 100 °C, which is lower than the required temperature to remove all the physisorbed water (i.e., 190 °C). In our previous work [4], the influence of the process conditions on the SSA of nano-silica synthesized by the dissolution of olivine was studied. We found that the SSA can be tailored in the range 90–400 m^2/g by changing the process conditions and applying Ostwald ripening treatments. In spite of these findings, this study mainly focused on the specific surface areas, without paying attention to the pore size distribution method nor the pore size development.

Even though the studies about the porosity of silica below the IEP have pointed out essential facts, more information is needed about the following topics in order to have a complete and detailed understanding of the pore structure development: 1) a reliable pore size distribution determination below 10 nm; 2) the influence of the reaction conversion and Ostwald ripening on the pore structure; and 3) a comprehensive model about the pore structure development.

In this article the development of the pore structure of nano-silica below the isoelectric point is studied by dissolving olivine in acid. Nitrogen physisorption and positron annihilation lifetime spectroscopy (PALS) were employed to determine the pore structure in the whole pore range. Furthermore, NMR analyses are performed to calculate the silanol content and SSA_{NMR}. Combining all these results, a better understanding about the pore structure development of silica below the IEP is obtained and a model is proposed.

2. Materials and methods

Precipitated nano-silicas were produced by dissolving a stoichiometric amount of olivine in sulfuric acid 3M in the temperature range of 50–90 °C as described by the following reaction and by a schematic diagram in the supporting information:

$$(Mg, Fe)_2SiO_4 + 4H^+ \rightarrow Si(OH)_4 + 2(Mg, Fe)^{2+}. \quad (1)$$

The dissolution yields a slurry of magnesium and iron salts, amorphous silica and unreacted minerals. Silica can, then, be cleaned by decantation and by washing/filtration as was described in our previous work [3,25].

The main experimental conditions that are modified in this work are the washing and filtration conditions, reaction time and Ostwald ripening conditions. The washing and filtration methods used were either consecutive filtration steps using vacuum filtration (P_{abs} = 0.2 bar) or a filter press (P_{abs} = 5 bar), where water was flushed continuously until a clean filtrate was obtained. The Ostwald ripening experiments were performed with a silica cake with a solid content of 20 wt%. These tests were carried out at different pH values between 4 and 11 at either 20 °C or 90 °C, these two parameters having a great influence in the solubility of silica. A high shear mixer (Silverson multifunctional L5M laboratory mixer with a shear screen) and a conventional mixer were used. The resulting silica samples were filtered and dried in an oven at 110 °C for about 15 h.

All samples were analyzed to determine their pore structure and SSA_{NMR}. The pore structure was determined by nitrogen physisorption and positron annihilation lifetime spectroscopy (PALS). A Micromeritics TriStar 3000 equipment using nitrogen as adsorbent at 77 K. Prior to the analysis, the samples were degassed for 240 min at 190 °C [26]. Using the BET method [27] (determined in p/p_0 range between 0.05 and 0.2) and the t-plot method (determined in p/p_0 range between 0.35 and 0.5) [28]. The SSA_{BET} and SSA_{MP} (Specific area in the micropores) were determined respectively. An external surface area (SSA_E) was calculated as the difference between SSA_{BET} and SSA_{MP}. The BJH method [29] was used to determine the pore size distribution, the pore volume (V_P) and the average pore diameter (d_P) from the desorption branch. The BJH method is used in the pore range between 2 and 300 nm, therefore, micropores are not taken into account using this procedure.

The PALS equipment used here consists of a positron source and a digital oscilloscope-based system employing photomultiplier tubes with BaF_2 scintillators at room temperature. The time resolution of the system is 200 ps full width at half maximum. For each spectrum at least 10^6 coincident counts are registered (more information about this method can be found in Refs. [30,31]). After subtracting the background, positron lifetime spectra are numerically analyzed by the POSITRONFIT code [32].

The solid state ^{29}Si MAS NMR spectra was obtained using a 400 Bruker Avance III spectrometer, operating at 79.5 MHz and a spinning rate of 10 KHz. The spectra were obtained after irradiating the samples with a $\pi/2$ (5 μs) pulse. Tetramethylsilane (TMS) was used as the external standard.

2.1. Silanol content and NMR specific surface area

The specific surface area determined by the BET method [27] using nitrogen can lead to inaccurate results when the sample is microporous [13,22,23,26,33] due to the method itself and, in the case that the pores are small enough, to the impossibility of nitrogen to penetrate them. Another way to determine the SSA is from the content of silanols, considering that the content of the surface silanol groups is constant when silica is fully hydroxylated (α_{FH}):

$$SSA_{NMR} = \frac{\alpha_{OH}}{\alpha_{FH}} \cdot SSA_{BET}, \quad (2)$$

where α_{OH} is the silanol content determined from the silica NMR spectrum using the procedure of Leonardelli [34]. The SSA_{NMR} is an important parameter of the olivine nano-silica since it provides the specific surface area of a fully hydroxylated silica, being different than that of the SSA_{BET}. The SSA_{NMR} determines the total content of the silanol groups, taking into account the amount of silanols in the ultramicropores and internal silanols. However, these surface areas are not accessible or difficult to access, which makes them less useful from the point of view of some applications.

According to Zhuravlev [35], the maximum extent of hydroxylation of silica is around 4.9 OH/nm^2. Zhuravlev determined this constant using the deuterium method, which is limited to surface silanols, and the SSA_{BET} using krypton [35]. Furthermore, the internal silanols and the silanols in pores narrower than 1 nm were neglected. Gallas [36], however, proposed a value of 8 OH/nm^2, where the silanol content was determined using TG-IR and the SSA_{BET} using nitrogen. Gallas attributed this difference in the silanol content to the fact that Zhuravlev used a surface area higher than expected, resulting in higher values of SSA_{BET} and lower values of α_{OH} [35,36]. In this work, a value of α_{FH} of 5 OH/nm^2 is used in Eq. (2) for the estimation of SSA_{NMR}, because this is the most widely used silanol value for fully hydroxylated silicas [19,35].

Table 1
Main properties of nano-silicas with different filtration steps.

Samples	SSA_{BET} (m^2/g)	SSA_{MP} (m^2/g)	SSA_E (m^2/g)	d_P (nm)	V_{MP} (cm^3/g)	V_P (cm^3/g)	S (%)	X (%)
NS1-3F	233	58	175	14.4	0.025	0.529	1.75	91
NS1-4F	324	122	202	12.6	0.055	0.578	0.33	91
NS1-5F	342	142	200	14.5	0.064	0.589	0.05	91
NS1-6F	348	142	206	16.3	0.064	0.679	0.03	91
NS2-HP	433	125	308	14.1	0.055	1.026	1.26	91

NS1 are filtered under vacuum and NS2 are filtered with a filter press. Where NS1-3F was filtered 3 times.

3. Results

3.1. Textural properties of olivine nano-silica using N_2 physisorption

The textural properties of the silica samples using different synthesis conditions were studied using nitrogen physisorption (the adsorption isotherms are provided in the supporting information). These properties are the specific surface areas (SSA_{BET}, SSA_{MP} and SSA_E), average pore size calculated (d_P), BJH volume of pores (V_P), and micropore volume (V_{MP}) calculated using the t-plot method. Furthermore, the sulfur content and the conversion (X) of the olivine dissolution reaction (see Eq. (1)) were also determined.

The number of washing and filtration steps have an important effect on the properties of this type of nano-silica. The sulfur content of NS-1-3F and 6F was reduced from 1.75 wt% to 0.03 wt% by adding three additional washing steps, and the SSA_{BET} increased from 233 m^2/g to 348 m^2/g (see Table 1). The pore size distribution in these two samples was similar, featuring pores between 2 nm and 100 nm (see Fig. 1a). On the other hand, the pore volumes were larger for samples with lower sulfate content. The sample with 6 filtration steps resulted in a 28% and 155% larger pore (meso and macropore) volume and micropore volume, respectively (see Fig. 1b). The higher increase in the micropore volume is because impurities are mainly located in them as we confirmed in Ref. [4]. On the other hand, the PSD of a sample filtered at high pressure (5 bars) was between 4 nm and 30 nm (See Fig. 2), showing a narrow peak and high pore volume around 20 nm, resulting in a sample without macroporosity. Therefore, the high filtration pressure can affect the porosity structure and in turn the SSA_{BET}.

The conversion (X) of the olivine dissolution reaction also has an impact on the textural properties of nano-silica as can be seen in Table 2. The PSD for the lowest conversion (NS3) was between 2 and 50 nm with a high pore volume around 15 nm. For samples with conversions above 75%, the pore sizes were in the range between 2 and 100 nm (see Fig. 3). That means that macroporosity is not present at the beginning of the reaction, but it is developed with time. The micropore volume remains almost constant independently of the reaction conversion (see Fig. 4). On the other hand, the pore volume decreases significantly with the conversion, meaning that the material is getting more compact (see Fig. 4).

The influence of the Ostwald ripening was studied at different pHs

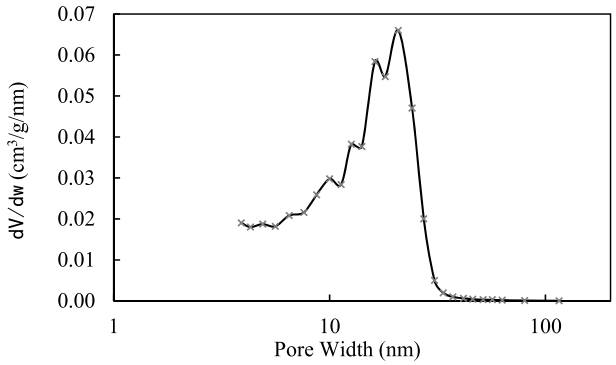

Fig. 2. Pore size distribution for NS2-HP.

Table 2
Main properties of nano-silicas at different reaction conversions.

Samples	SSA_{BET} (m^2/g)	SSA_{MP} (m^2/g)	SSA_E (m^2/g)	d_P (nm)	V_{MP} (cm^3/g)	V_P (cm^3/g)	S (%)	X (%)
NS3-S1	517	137	380	9.5	0.059	0.992	0.20	38
NS3-S2	325	132	193	12.9	0.060	0.597	0.33	77
NS3-S3	310	139	171	12.6	0.063	0.475	0.16	90
NS4-S1	375	124	251	13.7	0.055	0.816	0.40	81
NS4-S2	354	143	210	12.4	0.065	0.588	0.05	94

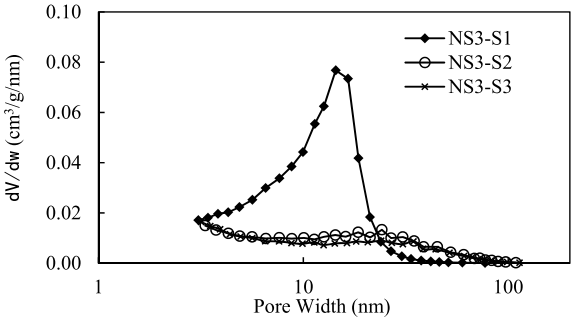

Fig. 3. Pore size distribution for silicas at conversions of 38, 77 and 90%.

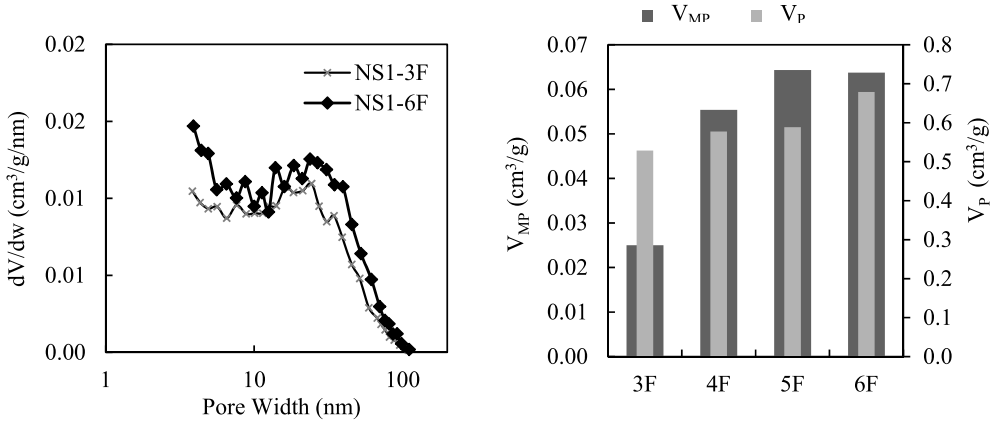

Fig. 1. Textural properties of silicas using different filtration steps: a) pore size distribution and b) micropore volume and pore volume.

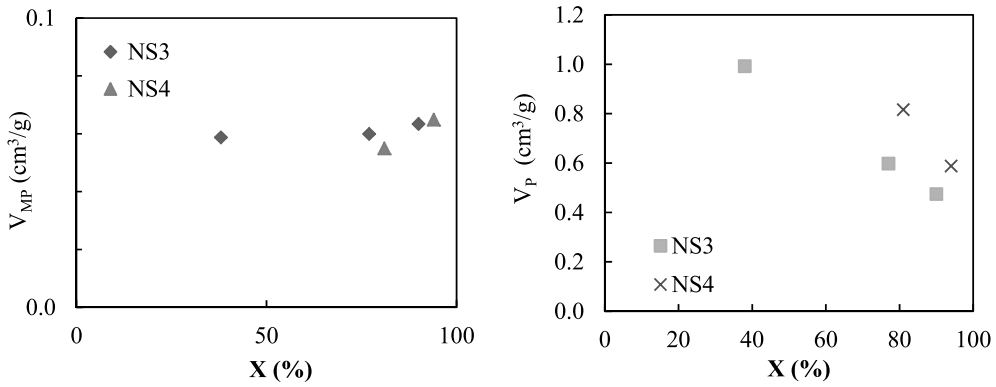

Fig. 4. Pore volumes versus the conversion degree for NS3 and NS4: a) the micropore volume and b) the pore volume.

Table 3
Main properties of nano-silicas after Ostwald ripening.

Samples	T (°C)	pH	SSA_{BET} (m^2/g)	SSA_{MP} (m^2/g)	SSA_E (m^2/g)	d_P (nm)	V_{MP} (cm^3/g)	V_P (cm^3/g)
NS5-RM	–	–	334	100	235	17.2	0.042	0.970
NS6	90	8.4	124	19	105	16.3	0.008	0.439
NS7	RT	4.6	347	105	242	16.6	0.046	0.969
NS8	RT	7.1	283	70	212	18.8	0.030	1.026
NS9	RT	9	191	26	165	25.2	0.010	1.003
NS10	RT	11	90	12	79	25.7	0.004	0.581

NS5-RM refers to the raw material used in the Ostwald ripening experiments. NS-6 was treated for 22 h using a conventional mixer and the rest of the samples were treated using a HM during 1 h.

(up to 11), at temperatures between 20 and 90 °C and using conventional or high shear mixers (see Table 3). The raw material nano-silica (NS5-RM) and the silica treated at 90 °C, at pH 8.4 and using a conventional mixer (NS6) featured a pore size distribution between 2 and 100 nm, but the pore volume was much lower in the ripened sample (see Table 3 and Fig. 5). The PSD of the sample treated at pH 11 using a high shear mixer (NS10) was in the range of 9–80 nm, with the porosity below 9 nm being completely removed (see Fig. 5). In addition, the micropore volume of this sample was almost negligible. The microporosity volume is reduced further and faster than the pore volume related to mesoporosity and macroporosity as the pH is increased. The pore volume remained constant for samples NS-7, -8 and, -9 and only decreased for NS-10 when the microporisity was already removed (see Fig. 5b).

The textural properties were also determined at 120 °C in order to study the degassing temperature influence (see Fig. 6). Silicas degassed at 190 °C featured higher micropore volumes than silicas degassed at 120 °C in agreement with the findings of Carrott [16], who stated that the volume of the micropores of precipitated silica increased with the degassing temperature up to 200 °C. Bergna [37] explained that this phenomenon is the result of the removal of adsorbed water from fully hydroxylated microporous surfaces. On the other hand, the degassing temperature has little or no influence on the pore volume.

3.2. Pore size measured by positron annihilation spectroscopy

The positron lifetime annihilation spectroscopy (PALS) technique measures the pore size and the pore intensity, which is related to the quantity of pores. Thus, samples with higher intensities have larger amount of pores. In the case of olivine nano-silica, pores of 6 Å (P1) and 25 Å (P2) were found. The pore size and pore intensity determination of P2 is just above the limit (20 Å) of the Tao-Eldrup model [38]. Therefore, the results of P2 are likely to feature a small error. P1 is considered an ultramicropore [22], while P2 is considered a small mesopore [39].

The influence of the process conditions on P1 is negligible; however, they have a significant effect on the intensity of P2, but not on the size. One way to explain the origin of these pores could be that P1 is intrinsic to the amorphous matrix of olivine nano-silica, remaining always constant, and P2 is related to the voids between the primary particles and influence by the process conditions. The intensity of P2 clearly decreases with the sulfur content (see Fig. 7a). This is because the sulfate salts are located in these pores, confirming our previous findings [4]. The intensity pronouncedly decreases with the conversion degree as can be seen in Fig. 7b, meaning that low range mesoporosity is greatly reduced. As the SSA_{BET} is reduced during the Ostwald ripening, the P2 intensity is reduced (see Fig. 7c), the decrease of the pore intensity being more pronounced for SSA_{BET} below 200 m^2/g.

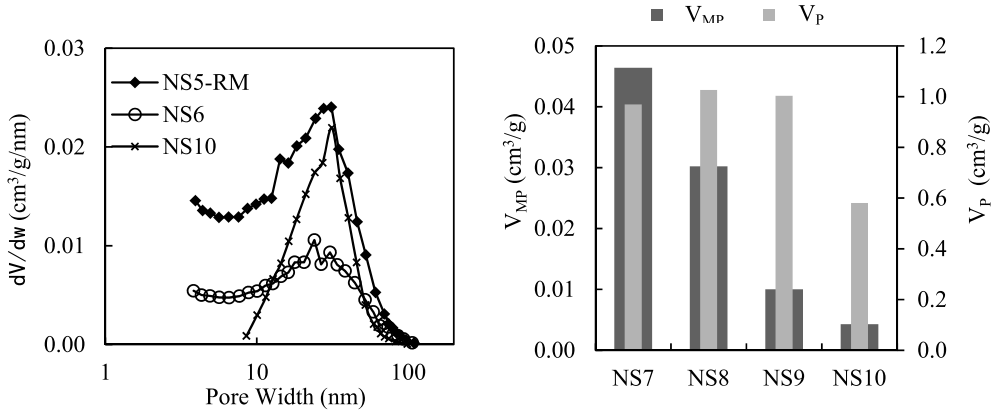

Fig. 5. Textural properties of Ostwald ripening silicas: a) pore size distribution and b) micropore volume and pore volume.

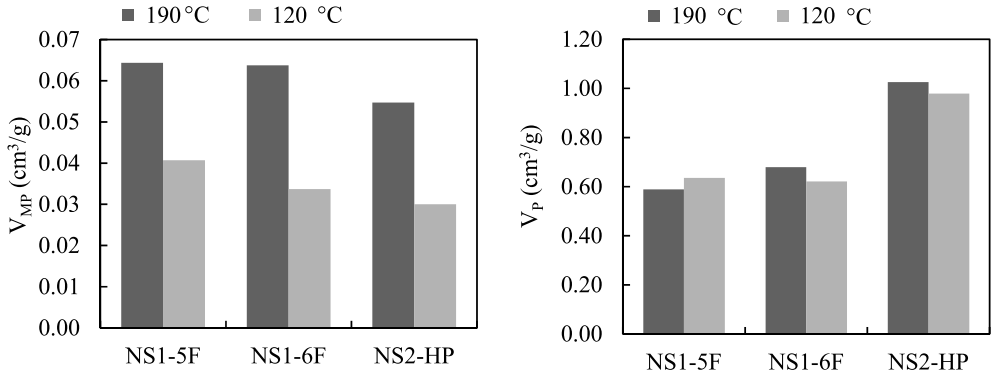

Fig. 6. Pore volumes for different silicas degassed at 190 and 120 °C: a) the micropore volume and b) the pore volume.

3.3. Silanol content and specific surface area measured by NMR

Silicas prepared from an aqueous route are always considered fully hydroxylated silica, with the silica surface completely covered by hydroxyl groups, featuring a silica content around 5 OH/nm^2 [35]. Using this value and Eq. (2), the SSA_{NMR} of the prepared silicas was calculated. The silanol number was also calculated from thermogravimetric analysis to compare them with the results obtained from NMR (see supporting information). Both determinations show similar results, the silanol content from TG analysis being slightly lower than that from NMR analysis.

When silicas are prepared using different filtration steps, the silanol content decreases with the SSA_{BET}, being in the range 8–15 OH/nm^2 (see Table 4 and Fig. 9a). This value is higher than the values obtained by Zhuralev (4.9 OH/nm^2) [35] and Gallas (~8 OH/nm^2) [36], but in the same range as the values reported by Lieftink (9–27 OH/nm^2) [19], especially if we consider that Lieftink dried its material at 100 °C. The reason for these high silanol values is because the NMR technique determines the total amount of silanols, including silanols in the ultramicropores and internal silanols, but the SSA_{BET} does not take into account the internal surface area nor the area of micropores. Therefore, high silanol values are indicative of either internal porosity (also called closed porosity) or ultramicropores. Additionally, the presence of ultramicropores of 6 Å was also confirmed in the PALS analyses and the presence of closed porosity can be observed in TEM pictures of this type of nano-silica (see Fig. 8).

The SSA_{NMR} presents values in the range between 650 and 800 m^2/g showing a slightly upward linear trend, which means that the factors (i.e., process conditions) affecting the SSA_{BET} also have a positive influence, though minimal, on the SSA_{NMR} (see Fig. 9b). We also found that the silanol content increases with the reaction conversion, whereas the SSA_{NMR} remains almost constant with it (see Fig. 10 and Table 5). This can be explained considering that as the conversion progresses, the silica particles grow in size developing internal porosity, which is computed in the SSA_{NMR} but not in SSA_{BET}.

Table 4
Silanol number and SSA_{NMR} for silicas with different filtration methods.

Samples	X (%)	S (%)	SSA_{BET} (m^2/g)	α_{OH} (OH/nm^2)	α_{OH}/α_{FH}	SSA_{NMR} (m^2/g)
NS1-3F	91	1.75	233	14.3	2.9	668
NS1-6F	91	0.03	343	10.9	2.2	745
NS2-HP	91	1.26	433	8.9	1.8	773

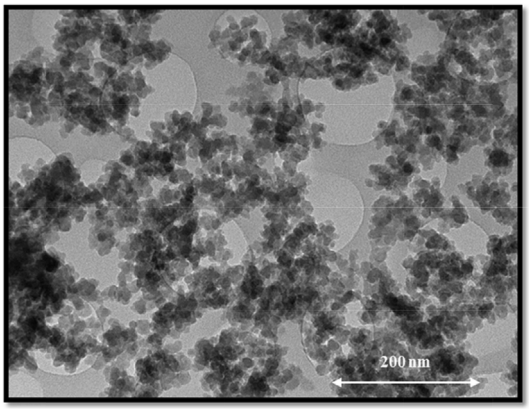

Fig. 8. TEM picture of NS1-6F.

The silanol content for ripened silicas rises as the SSA_{BET} is reduced due to the Ostwald treatment (Fig. 11a and Table 6), 40 OH/nm^2 being the highest silanol values obtained for the sample with the lowest SSA_{BET} and most intensive treatment (NS10). This value is eight times higher than the one silanol content proposed by Zhuralev [35] for fully hydroxylated silica and this is due to the relative increase of silanols in the internal pores. This phenomenon occurs because the SSA_{BET} is reduced drastically with the Ostwald ripening, but the SSA_{NMR} remains

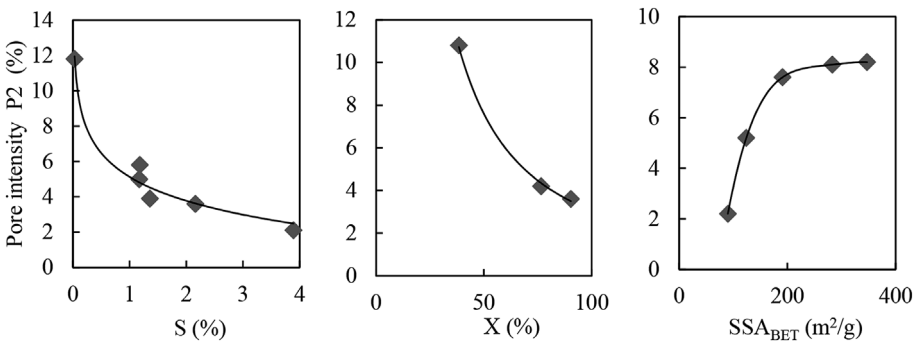

Fig. 7. Intensity of P2 versus a) sulfur content, b) reaction conversion and c) SSA_{BET} in the ripened silicas.

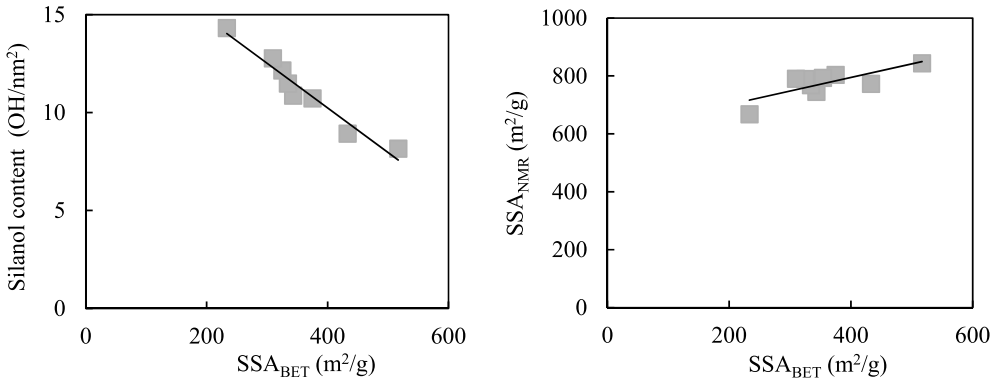

Fig. 9. a) Silanol content versus SSA_{BET}. b) SSA_{NMR} versus SSA_{BET}.

Table 5
Silanol number and SSA_{NMR} for silicas with different reaction conversions.

Samples	X (%)	S (%)	SSA_{BET} (m^2/g)	α_{OH} (OH/nm^2)	α_{OH}/α_{FH}	SSA_{NMR} (m^2/g)
NS3-S1	38	0.20	517	8.2	1.6	844
NS3-S2	77	0.33	325	12.1	2.4	790
NS3-S3	90	0.16	310	12.8	2.6	791
NS4-S1	81	0.40	375	10.7	2.1	804
NS4-S2	94	0.05	354	11.2	2.2	793

almost constant, only slightly decreasing with the treatment (see Fig. 11b). Actually, the most intensive treated sample (i.e., NS10) features 8 times more SSA_{NMR} than SSA_{BET}, while in the initial raw material is not more than doble.

4. Pore structure development

Prior to analyzing how the pore structure develops with the reaction conversion, a few aspects about the particle growth of silica should be recalled since pore structure mainly depends on the particle growth development and particle structure. The particle growth of silica below the IEP with a continuous release of silica monomers into the medium can be summarized as described in our previous work [40]: Soluble silica nucleates and primary particles around 3 nm are formed. The silica particles grow mainly by aggregation, forming linear chains. As the growth continues, the silica chains keep increasing in size, and at a certain moment, branching starts to occur forming 3D network aggregates, which agglomerate with time forming final particles as large as (or even larger) one μm. This particle growth development is schematically represented in Fig. 12 together with a TEM picture of the final agglomerates.

Compactation of the pore structure and internal porosity can be observed at the highest reaction conversion. Development of macroporosity is not represented here because the agglomerates are too big for the adopted scale.

The SSA_{BET} and pore volume are greatly influenced by the reaction conversion, decreasing with X (see Fig. 13). SSA_{BET} shows a similar trend to V_P since SSA_{BET} is the sum of SSA_E, which is related to the pore volume, and SSA_{MP}, which according to the PALS results (P1) remains constant during the synthesis process. The decrease of V_P can also be inferred from Fig. 3, which shows that the pore size distribution is wider, but much flatter for higher conversion degrees. The decrease of the pore volume with conversions means that the silica agglomerates become more compact due to a better packing of the particles, which is also confirmed by the intensity decrease of P2 by PALS. This is in agreement with the findings of Okkerse [41], who stated that a better packing was obtained for silicas gels after longer gelling times. This packing improvement is also represented in our previous particle growth model (see Fig. 12). Another interesting fact from the PSD is that at the beginning of the reaction, the silica is only microporous and mesoporous, and as the reaction progresses, macroporisity is developed, which is in agreement with the findings of Lieftink [19]. A possible explanation for this phenomenon is that at the beginning, the aggregates are small; therefore, pores should be smaller. As the aggregates grow, which they do via random collision [40], silica particles become much larger than 50 nm and macroporosity can be formed. It is noteworthy, that even though macropores are developed, particles become more compact featuring a lower pore volume and SSA_{BET}.

The SSA_{NMR} decreases slightly with the reaction conversion (see Fig. 13 and Table 5). This reduction occurs, but to a much lower extent than for SSA_{BET} and V_P. The difference in the reductions of SSA_{NMR} and SSA_{BET} could be explained assuming that internal porosity is developed as the particles grow (represented in Fig. 12). In addition, the silanols in the ultramicropores are likely to remain constant. In addition, the development of internal porosity is in agreement with random collision as the main particle growth mechanism as proposed in Ref. [40].

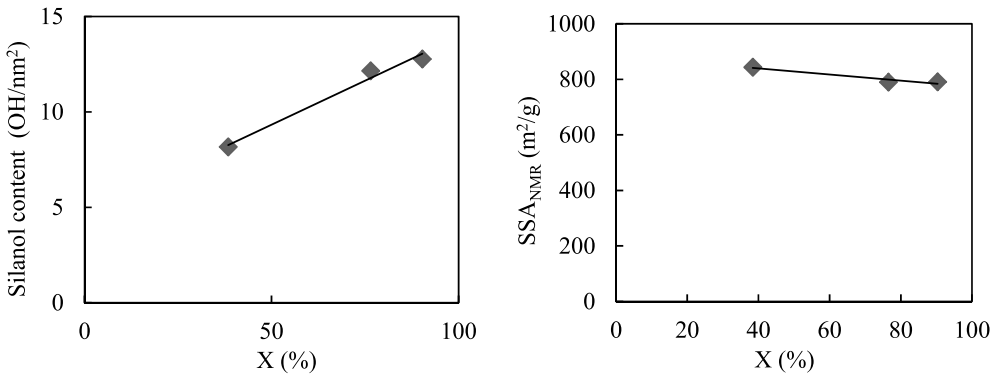

Fig. 10. a) Silanol content versus conversion degree for sample NS3. b) SSA_{NMR} versus conversion degree for NS3.

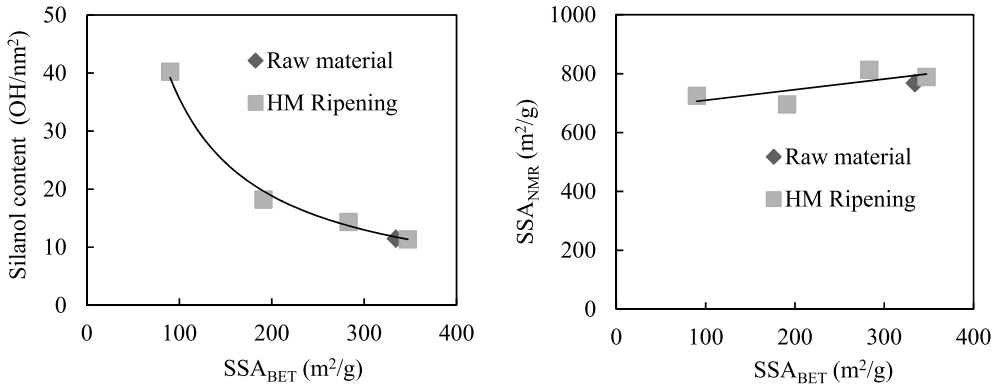

Fig. 11. a) Silanol content versus SSA_{BET} for ripened nano-silicas. b) SSA_{NMR} versus SSA_{BET} for ripened olivine nano-silicas. HM refers to samples prepared with the high shear mixer.

Table 6
Silanol number and SSA_{NMR} for Ostwald ripened nano-silicas.

Samples	SSA_{BET} (m^2/g)	α (OH/nm^2)	α_{OH}/α_{FH}	SSA_{NMR} (m^2/g)
NS5-RM[a]	334	11.5	2.3	768
NS6	124	22.2	4.4	551
NS7	347	11.4	2.3	789
NS8	283	14.4	2.9	814
NS9	191	18.2	3.6	696
NS10	90	40.3	8.1	725

[a] Where NS5-RM was obtained with an X > 90% and the sulfur content was 0.06%.

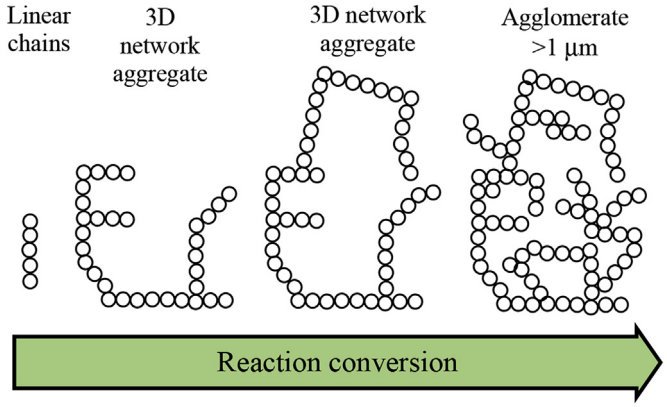

Fig. 12. a) Schematic particle growth model (adapted from Ref. [40]) and b) TEM pictures of silica produced below the IEP.

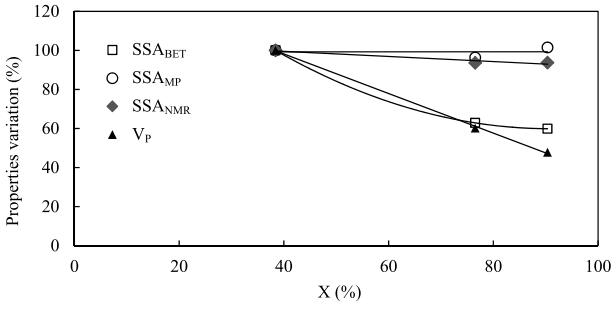

Fig. 13. Variation of the textural properties of olivine nano-silica versus the reaction conversion.

The Ostwald ripening has also a great influence on the textural properties of silica. The general trend is that the SSA and pore volume decrease as the pH of the treatment is increased (see Fig. 14). The

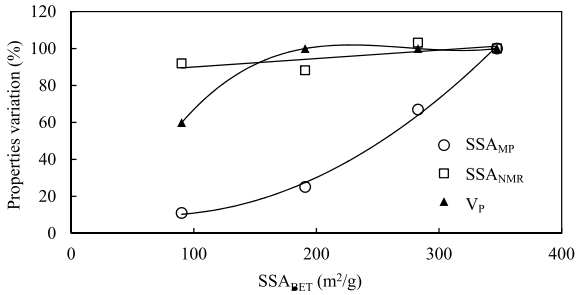

Fig. 14. Variation of the textural properties of ripened olivine nano-silica versus the SSA_{BET}.

largest decrease takes place on the SSA_{MP} with a decrease up to 90% at pH 11. This pronounced decrease of SSA_{MP} is due to the reduction of pores of around 2 nm as can be inferred from the PALS results, where the P2 intensity decreased by 75% (see Fig. 7). Therefore, the microporosity was reduced significantly, but the ultramicropores remained unaffected. The pore volume remained constant for non-intensive ripening treatments, decreasing for samples with a SSA_{BET} below 200 m^2/g. The pore range was also reduced for intensive treatment (see Fig. 5b), the pores below 9 nm being completely removed for treatments at pH 11. This phenomenon is because: 1) the solubility of silica increases exponentially with pH [13] and 2) dissolved silica condensates initially on the walls of accessible micropores, and when most of the micropores have been filled, the dissolved silica condensates on the smaller mesopores. The SSA_{NMR} decreases gradually and slowly with the ripening treatment, resulting in a total reduction of 8% for the most intensive ripening. This small reduction is most likely due to the fact that the Ostwald ripening does not have an influence in internal surface area and in the ultramicropores.

5. Conclusions

Nano-silica synthesized by the dissolution of olivine, which is a sustainable alternative to the existing commercial methods, exhibits a SSA_{BET} in the range of 100–500 m^2/g and a pore size distribution between 1 and 100 nm for silicas of high purity. At the beginning of the reaction, silica is microporous and mesoporous, showing no macroporosity. As the reaction conversion progresses, silica particles become larger forming 3D networks through collision of random particles and macroporous and internal porosity are developed. On the other hand, even though the final particles are still highly porous, some degree of internal rearrangement must take place since particles become more compact.

Two types of pores were found in this material using positron annihilation lifetime spectroscopy: one at around 6 Å and another one at

around 25 Å. Pore 1 is an ultramicropore and can be considered to be intrinsic to the amorphous matrix of olivine nano-silica (unaffected by the process conditions), and pore 2 is a small mesopore and is likely due to the voids between the primary particles, being significantly affected by the process conditions. The findings presented here are based on our results dissolving olivine in acid, but they could also be applied under any other circumstances where silica is released into the medium below the IEP.

The synthesis process conditions have an important influence on the textural properties of olivine nano-silica. The process conditions can be modified by changing the filtration pressure, controlling the reaction conversion and/or performing Ostwald ripening treatments. Thus, the initial pore size distribution (1–100 nm) can be tailored to distributions where the small mesopores can be removed featuring no porosity below 9 nm (except for the ultramicropores of 6 Å which they remain constant) and the large pores can be reduced to pore sizes as small as 30 nm. The possibility of tailoring the porosity of silica in this large range makes this material suitable for a wide range of applications.

Acknowledgement

The authors wish to express their appreciations to Mr Q. Alam and Mr J. Nokes for the fruitful discussions and comments and to the Dutch Technology Foundation STW for sponsoring this project (Project 12824 - Tailoring new nano-silica, and its application in smart concrete). They furthermore express their gratitude to to the following sponsors of the Building Materials research group at TU Eindhoven: Rijkswaterstaat Grote Projecten en Onderhoud; Graniet-Import Benelux; Kijlstra Betonmortel; Struyk Verwo; Attero; Enci; Rijkswaterstaat Zee en Delta-District Noord; Van Gansewinkel Minerals; BTE; V.d. Bosch Beton; Selor; GMB; Geochem Research; Icopal; BN International; Eltomation; Knauf Gips; Hess AAC Systems; Kronos; Joma; CRH Europe Sustainable Concrete Centre; Cement & Beton Centrum; Heros; Inashco; Keim; Sirius International; Boskalis; NNERGY; Tata Steel; Millvision; Sappi; Studio Roex and Van Berlo Groep (in chronological order of joining).

Appendix A. Supplementary data

Supplementary data related to this article can be found at http://dx.doi.org/10.1016/j.micromeso.2018.03.031.

References

[1] Freedonia, World Specialty Silicas, (2016).
[2] W. Stöber, A. Fink, E. Bohn, J. Colloid Interface Sci. 26 (1968) 62–69.
[3] A. Lazaro, H.J.H. Brouwers, G. Quercia, J.W. Geus, Chem. Eng. J. 211–212 (2012) 112–121.
[4] A. Lazaro, M.C. Van de Griend, H.J.H. Brouwers, J.W. Geus, Microporous Mesoporous Mater. 181 (2013) 254–261.
[5] A. Lazaro, G. Quercia, H.J.H. Brouwers, J.W. Geus, World J. Nano Sci. Eng. 3 (2013) 41–51.
[6] H. Wu, B. Tang, P. Wu, J. Phys. Chem. C 116 (2012) 2246–2252.
[7] A. Corma, Chem. Rev. 97 (1997) 2373–2420.
[8] I.I. Slowing, J.L. Vivero-Escoto, C.W. Wu, V.S.Y. Lin, Adv. Drug Deliv. Rev. 60 (2008) 1278–1288.
[9] P.A. Bazula, P.M. Arnal, C. Galeano, B. Zibrowius, W. Schmidt, F. Schüth, Microporous Mesoporous Mater. 200 (2014) 317–325.
[10] J. Liu, Q. Yang, X.S. Zhao, L. Zhang, Microporous Mesoporous Mater. 106 (2007) 62–67.
[11] D.A. Kurdyukov, D.A. Eurov, D.A. Kirilenko, J.A. Kukushkina, V.V. Sokolov, M.A. Yagovkina, V.G. Golubev, Microporous Mesoporous Mater. 223 (2016) 225–229.
[12] D.A. Kurdyukov, D.A. Eurov, D.A. Kirilenko, V.V. Sokolov, V.G. Golubev, Microporous Mesoporous Mater. 258 (2018) 205–210.
[13] R.K. Iler, The Chemistry of Silica: Solubility, Polymerization, Colloid and Surface Properties, and Biochemistry, John Wiley and Sons, 1979.
[14] F. Ehrburger-Dolle, M. Holz, C. Mauzac, J. Lahaye, G.M. Pajonk, J. Non-Cryst. Solids 145 (1992) 185–190.
[15] M.K. Titulaer, M.J. den Exter, H. Talsma, J.B.H. Jansen, J.W. Geus, J. Non-Cryst. Solids 170 (1994) 113–127.
[16] P.J.M. Carrott, K.S.W. Sing, Adsorpt. Sci. Technol. 1 (1984) 31–39.
[17] C.T. Kresge, M.E. Leonowicz, W.J. Roth, J.C. Vartuli, J.S. Beck, Nature 359 (1992) 710–712.
[18] F. Shi, L. Wang, J. Liu, Mater. Lett. 60 (2006) 3718–3722.
[19] D.J. Lieftink, The Preparation and Characterization of Silica from Acid Treatment of Olivine, Utrecht University, 1997 PhD Thesis.
[20] C. Okkerse, Submicroporous and Macroporous Silica, Delft University of Technology, 1961 PhD Thesis.
[21] R. Denoyel, M. Barrande, I. Beurroies, Studies in Surface Science and Catalysis, (2007), pp. 33–40.
[22] S. Lowell, J.E. Shields, M.A. Thomas, M. Thommes, Characterization of Porous Solids and Powders: Surface Area, Pore Size and Density vol. 16, Springer, 2006.
[23] M.C. Duke, S.J. Pas, A.J. Hill, Y.S. Lin, J.C.D. da Costa, Adv. Funct. Mater. 18 (2008) 3818–3826.
[24] A.V. Neimark, P.I. Ravikovitch, M. Grün, F. Schüth, K.K. Unger, J. Colloid Interface Sci. 207 (1998) 159–169.
[25] A. Lazaro, L. Benac-Vegas, H.J.H. Brouwers, J.W. Geus, J. Bastida, Appl. Geochem. 52 (2015) 1–15.
[26] ISO 9277, Determination of the Specific Surface Area of Solids by Gas Adsorption - BET Method, 2010, (2010).
[27] S. Brunauer, P.H. Emmett, E. Teller, J. Am. Chem. Soc. (1938) 309–319.
[28] J.H. de Boer, B.C. Lippens, B.G. Linsen, J.C.P. Broekhoff, A. van den Heuvel, T. Osinga, J. Colloid Interface Sci. 21 (1966) 405–414.
[29] E.P. Barrett, L.G. Joyner, P.P. Halenda, J. Am. Chem. Soc. (1951) 373–380.
[30] K. Sato, K. Fujimoto, M. Nakata, T. Hatta, J. Phys. Chem. C 115 (2011) 18131–18135.
[31] K. Sato, J. Phys. Chem. B 115 (2011) 14874–14877.
[32] P. Kirkegaard, M. Eldrup, Comput. Phys. Commun. 7 (1974) 401–409.
[33] S. Brunauer, J. Colloid Interface Sci. 41 (1972) 612–614.
[34] S. Leonardelli, L. Facchini, C. Fretigny, P. Tougne, A.P. Legrand, J. Am. Chem. Soc. 114 (1992) 6412–6418.
[35] L.T. Zhuravlev, Colloid. Surface. Physicochem. Eng. Aspect. 173 (10-11-2000) 1–38.
[36] J.P. Gallas, J.M. Goupil, A. Vimont, J.C. Lavalley, B. Gil, J.P. Gilson, O. Miserque, Langmuir 25 (2009) 5825–5834.
[37] H.E. Bergna, W.O. Roberts, Colloidal Silica: fundamentals and Applications 131 CRC, 2006.
[38] K. Ito, H. Nakanishi, Y. Ujihira, J. Phys. Chem. B 103 (1999) 4555–4558.
[39] K.S.W. Sing, D.H. Everett, R.A. Haul, L. Moscous, R.A. Pierotti, J. Rouquerol, T. Siemieniewska, Pure Appl. Chem. (1985) 603–619.
[40] A. Lazaro, N. Vilanova, L.D. Barreto Torres, G. Resoort, I.K. Voets, H.J. Brouwers, Langmuir 33 (2017) 14618–14626.
[41] C. Okkerse, Porous silica, in: Linsen, G. Bastiaan (Eds.), Physical and Chemical Aspects of Adsorbents and Catalysts, Academic Press, 1970, pp. 213–264 [5].